Counter-anions-tuned crystal structure and intermolecular interactions of a series of iron (II) complexes derived from 4,4'-dimethyl-2,2'-bipyridine

Li-Jing Yang, Qing-Ling Liu, Yang-Hui Luo, Wei Wang, Yang Ling, Gang Yao & Bai-Wang Sun

Taylor & Francis
Taylor & Francis Group

Counter-anions-tuned crystal structure and intermolecular interactions of a series of iron (II) complexes derived from 4,4′-dimethyl-2,2′-bipyridine

Li-Jing Yang[a], Qing-Ling Liu[a], Yang-Hui Luo[a], Wei Wang[a], Yang Ling[a], Gang Yao[b], and Bai-Wang Sun[a]

[a]School of Chemistry and Chemical Engineering, Southeast University, Nanjing, P. R. China; [b]College of Chengxian, Southeast University, Nanjing, P. R. China

ABSTRACT

A series of Fe(II) complexes with $(ClO_4)^-(SeCN)^-$, $(ClO_4)^-(SCN)^-$, $(Fe_2OCl_6)^{2-}$, and $2(BF_4)^-$ counter-anions for complexes **1–4**, derived from dmbpy (4,4′-dimethyl-2,2′-bipyridine), were prepared. The single-crystal studies and the Hirshfeld surfaces analysis revealed that the $(Fe_2OCl_6)^{2-}$ anion results more distortional octahedral geometry of the cation than other anions. In particular, the $(ClO_4)^-(SCN)^-$ and $(Fe_2OCl_6)^{2-}$ anions lead to complexes **2** and **3** stabilized via C-H···π interactions and π···π interactions, which were not found in the other two complexes. However, the double-chain structure of complex **4** was formed by C-H···F and C-H···C hydrogen bonds interactions. Due to the influence of different anions, magnetic susceptibility measurements showed that complex **1** was in high-spin (HS) state and complex **2** was in low-spin (LS) state.

Introduction

Substituted 2,2′-bipydine ligands, for example, 4,4′-dimethyl-2,2′-bipyridine (dmbpy) and its derivatives, which serve as bi-dentate ligands, are very useful ligands capable to construct abundant coordination complexes with different oxidation state metals, such as Cu(II), Ag(I), Pd(II), In(III), Fe(II), etc. [1–9] These complexes, which were derived from dmbpy and its derivatives, have been attracting great interest of researchers for many years because of their fascinating molecular structures and novel properties, such as spectroscopic, catalytic, magnetic, and biological properties, in a variety of areas [1, 6].

In the past decades, many efforts have been made to synthesize and investigate the iron(II) (3d^6) complexes for their magnetic behavior and in respect of the phenomenon of spin-crossover. These Fe(II) complexes can be served as advanced materials used in sensory and memory devices [10, 11]. There are numerous reports about Fe(II) complexes, which contain one or two dmbpy ligands [12–14]. However, only few complexes that three dmbpy molecules coordinated to Fe(II) have been prepared. Huang and Ogawa [2a] reported a low-spin Fe(II) complex, formulated as [Fe(dmbpy)$_3$](NCS)$_2$·3H$_2$O, and in

Scheme 1. The preparation method for complexes **1–4**.

our previous work [15] we reported the first example of $[Fe(dmbpy)_3]^{2+}$ complex, namely $[Fe(dmbpy)_3](ClO_4)(SCN)\cdot 3H_2O$, a water free complex that exhibits spin-crossover properties.

In addition, some evidence shows that counter-anions can influence the structure, magnetism, catalyst reactivity, and the antimicrobial reactivity of metal complexes [16], and play vital roles in the construction of molecules [17]. In this study, four Fe(II) complexes **1–4** with different counter-anions (Scheme 1) have been synthesized, and the X-ray crystal structures were studied. What's more, the influence of different counter-anions on the structures, magnetic properties, and intermolecular interactions of these complexes was further investigated.

Experimental

Materials and measurements

All chemicals, obtained commercially, were of analytical grade and used without further purification. 4,4′-Dimethyl-2,2′-bipyridine (purity: ≥99%, CAS number: 1134-35-6) was purchased from Alfa Aesar, and other reagents were purchased from NanJing WanQing Chemical Glassware Instrument Co. Ltd.; all of these were used as received.

Elemental analyses of carbon, hydrogen, and nitrogen were performed with a Vario-EL III elemental analyzer. Dynamic scanning calorimetric (DSC) and thermogravimetric analyses (TGA) were performed using a Mettler–Toledo TGA-DSC STAR^e System in a nitrogen atmosphere in the range of 50–500°C, with a heating rate of 10 K·min^{-1}. The TGA–DSC dates were analyzed using STARe Software. Temperature-dependent magnetization (M-T) of complexes **1** and **2** was measured in the temperature range of 305–0 K in the fields of 2 kOe using a quantum design vibrating sample magnetometer in a physical property measurement system at a scan rate of 1 K/min. Measurements were performed on ground polycrystalline samples of 14.2 mg (**1**) and 15.5 mg (**2**). The magnetic data were corrected from the sample holder and diamagnetic contributions.

Synthesis and characterization

Synthesis of complex **1** {$[Fe(dmbpy)_3](ClO_4)(SeCN)$}: To a solution of $Fe(ClO_4)_2\cdot 6H_2O$ (0.073 g, 0.2 mmol) in MeOH (10 mL), a solution of KSeCN (0.058 g, 0.4 mmol) in MeOH (10 mL) was added. The mixture was added into MeOH solution containing dmbpy (0.111 g, 0.6 mmol) at a temperature of 25°C under continuous stirring. After stirring for about 30 min, the solution, which resulted from the mixture, was filtered off and allowed to evaporate at room temperature. The brown single crystals of complex **1** were grown from the solution by slow evaporation at room temperature in five days. Yield: 0.229 g (70%), based on Fe. Elemental analysis of complex **1**: Anal. Calcd. (%): C, 54.66; N, 12.06; H, 4.46. Found: C, 54.58; N, 12.02; H, 4.54.

Synthesis of complex **2** {[Fe(dmbpy)$_3$](ClO$_4$)(SCN)}: Complex **2** was prepared by a procedure similar to complex **1** but using KSCN (0.039 g, 0.4 mmol) instead of KSeCN. Brown single crystals of complex **2** were grown from the solution by slow evaporation at room temperature in five days. Yield 0.209 g (68%), based on Fe. Elemental analysis for complex **2**: Anal. calcd. (%): C, 58.00; N, 12.80; H, 4.74. Found: C, 58.08; N, 12.72; H, 4.79.

Synthesis of complex **3** {[Fe(dmbpy)$_3$](Fe$_2$OCl$_6$)}: To a solution of FeCl$_2$·4H$_2$O (0.040 g, 0.2 mmol) in MeOH (10 mL), solution of dmbpy (0.111 g, 0.6 mmol) in MeOH (10 mL) was added at a temperature of 25°C under continuous stirring. After stirring for about 30 min, the solution, which resulted from the mixture, was filtered off and allowed to evaporate at room temperature. Brown single crystals of complex **3** were grown from the solution by slow evaporation at room temperature in seven days. Yield 0.249 g (65%), based on Fe. Elemental analysis for complex **3**: Anal. Calcd. (%): C, 45.56; N, 8.86; H, 3.82. Found: C, 45.51; N, 8.78; H, 3.88.

Synthesis of complex **4** {[Fe(dmbpy)$_3$](BF$_4$)$_2$}: Complex **4** was prepared by a procedure similar to complex **3** but using Fe(BF$_4$)$_2$·4H$_2$O (0.060 g, 0.2 mmol) instead of FeCl$_2$·4H$_2$O. Brown single crystals of complex **4** were grown from the solution by slow evaporation at room temperature in four days. Yield 0.330 g (70%), based on Fe. Elemental analysis for complex **4**: Anal. Calcd. (%): C, 55.28; N, 10.74; H, 4.64. Found: C, 55.16; N, 10.79; H, 4.57.

X-ray crystallographic study

The single-crystal X-ray diffraction data of complexes **1**--**4** were collected at 293 K with graphite-monochromated Mo-Kα radiation (λ = 0.071073 nm), a Rigaku SCX mini-diffractometer with the ω-scan technique [18]. The lattice parameters were integrated using vector analysis and refined from the diffraction matrix, and the absorption correction was carried out by using Bruker SADABS program with a multi-scan method. Since the Crystallographic Information File (CIF) of complex **4** cannot be obtained, a summary of crystallographic data, data collection, and refinement parameters for complexes **1**–**3** are summarized in Table 1. The structures of these were solved by full-matrix least-square methods on all F^2 data, and used SHELXS-97 and SHELXL-97 programs [19] for structure solution and

Table 1. Crystal data and structure refinement for complexes **1**–**3**.

| Compound	1	2	3
Formula	C$_{37}$H$_{36}$FeN$_7$O$_4$ClSe	C$_{37}$H$_{36}$FeN$_7$O$_4$SCl	C$_{36}$H$_{36}$Fe$_3$N$_6$OCl$_6$
Formula weight	812.98	766.09	948.96
Crystal system	Monoclinic	Monoclinic	Monoclinic
Space group	C 2/c	C 2/c	P 21/c
a (Å)	11.750(2)	10.826(2)	19.498(4)
b (Å)	29.354(8)	27.438(8)	11.379(2)
c (Å)	15.400(3)	14.339(3)	20.607(4)
α	90°	90°	90°
β (°)	101.19(3)	102.70(3)	114.74(3)
γ	90°	90°	90°
V (Å^3)	5210(2)	4155.1(17)	4152.4(14)
Z	4	4	4
D$_{calc}$ (Mg m^{-3})	1.038	1.225	1.518
T (K)	293(2)	293(2)	293(2)
μ (mm^{-1})	1.074	0.528	1.457
Cryst dimensions	0.36×0.30×0.27	0.30×0.25×0.20	0.25×0.28×0.20
Goodness-of-fit on F^2	1.038	1.013	1.013
R_1, wR_2 ((I > 2σ(I)))	0.0620, 0.1814	0.1226, 0.1985	0.0961, 0.1968
R_1, wR_2 (all data)	0.0784, 0.1961	0.1411, 0.2125	0.2602, 0.2743
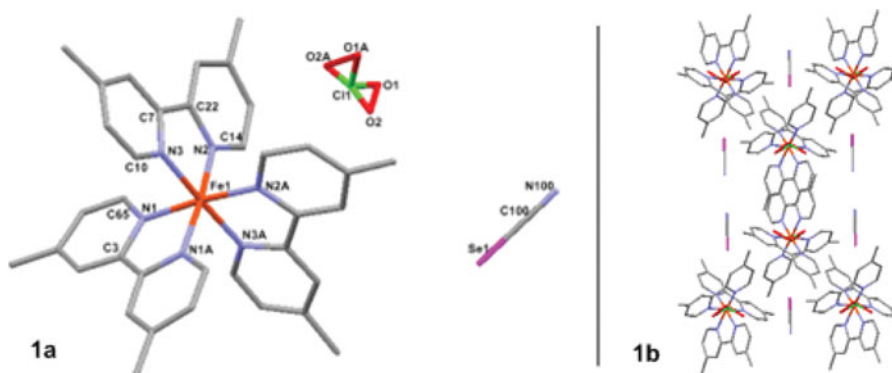
Figure 1. (a) Molecular structure and numbering scheme of complex **1**; **1b**: Packing diagram of complex **1** viewed along *c*-axis (H atoms are omitted for clarity).

structure refinement respectively. Reliability factors were defined as $R_1 = \Sigma(|Fo|-|Fc|)/\Sigma|Fo|$ and the function minimized was $Rw = [\Sigma w(Fo_2 - Fc_2)2/w(Fo)4]^{1/2}$, whereas in the least-square calculations the unit weight was used. All non-hydrogen atoms were refined anisotropically, and hydrogen atoms were inserted at their calculated positions and fixed at their positions [20]. The molecular graphics were prepared by Mercury [21].

Hirshfeld surfaces calculations

The molecular Hirshfeld surface (d_{norm}) calculations were performed by using CrystalExplorer program [22]. In this study, all the Hirshfeld surfaces were generated using a standard (high) surface resolution. The 3D d_{norm} surfaces were mapped over a fixed color scale of -0.42 (red) to 1.6 Å (blue), and the 2D fingerprint plots displayed by using the standard 0.6–2.6 Å view with the d_e and d_i scales displayed on graph axes.

Results and discussions

Crystal structure of complex 1

Complex **1** crystallizes as brown block crystals in the monoclinic *C*2/*c* space group with $Z = 4$, the asymmetric unit (ASU) contains half of the cation, which comprises one Fe^{II} ion, three dmbpy ligands, 1/2 dissociative ClO_4^- anion, and one $SeCN^-$ anion (Figure 1a). For cation, Fe^{II} ion shows a distorted octahedral geometry formed by six N atoms from three dmbpy receptors. The Fe-N bond lengths varied from 2.068(10) to 2.187(11) Å with an average value of 2.131(11) Å (Table 2), which is a typical value for the HS Fe^{II}-N bond lengths of mononuclear Fe^{II} complex, and the C-N bond lengths vary from 1.393(14) Å to 1.546(16) Å. The two pyridine rings of dmbpy are not coplanar with the dihedral angles between the same dmbpy of 4.56°, 8.85°, and 9.03° respectively. In addition, the bite angles of three dmbpy planes are 87.66, 81.30, and 80.91°.

Since the intermolecular distance is relatively too far, there is no molecular interactions between the adjacent molecules. The packing diagram of complex **1** like a "frog" is viewed along the *c*-axis (Figure 1b), and the $SeCN^-$ anions are evenly distributed in the head, tail, and both sides of the body, while the ClO_4^- anions are located in the trunk and the center of the legs.

Table 2. Selected bond lengths (Å) for complexes **1**–**4**.

	1		2		3		4	
Fe–N	Fe1-N1	2.137(10)	Fe1-N1	1.979(10)	Fe1-N19	1.977(6)	Fe7-N1	1.965(10)
	Fe1-N1A	2.114(10)	Fe1-N1A	1.979(10)	Fe1-N20	1.978(6)	Fe7-N2	1.922(10)
	Fe1-N2	2.068(10)	Fe1-N2	1.959(10)	Fe1-N21	1.963(6)	Fe7-N3	2.004(10)
	Fe1-N2A	2.092(10)	Fe1-N2A	1.959(10)	Fe1-N22	1.949(6)	Fe7-N4	1.947(10)
	Fe1-N3	2.186(11)	Fe1-N3	1.969(10)	Fe1-N23	1.965(6)	Fe7-N5	2.020(10)
	Fe1-N3A	2.187(11)	Fe1-N3A	1.969(10)	Fe1-N24	1.987(6)	Fe7-N6	1.992(10)
	Fe-N*av*	2.131(10)	Fe-N*av*	1.969(10)	Fe-N*av*	1.970(6)	Fe-N*av*	1.975(10)
N–C	N1-C65	1.463(14)	N1-C7	1.355(15)	N19-C33	1.370(9)	N1-C7	1.385(15)
	N1-C3	1.466(14)	N1-C12	1.425(15)	N19-C8	1.378(9)	N1-C12	1.353(15)
	N2-C14	1.494(16)	N2-C1	1.295(14)	N20-C11	1.336(9)	N2-C6	1.443(15)
	N2-C22	1.546(16)	N2-C6	1.394(16)	N20-C87	1.360(9)	N2-C1	1.303(15)
	N3-C10	1.393(14)	N3-C18	1.358(14)	N21-C7	1.337(9)	N3-C248	1.390(15)
	N3-C7	1.462(15)	N3-C13	1.325(14)	N21-C6	1.366(9)	N3-C245	1.310(15)
					N22-C3	1.356(9)	N4-C232	1.403(14)
					N22-C2	1.357(9)	N4-C250	1.353(14)
					N23-C9	1.343(9)	N5-C251	1.219(15)
					N23-C25	1.364(9)	N5-C249	1.366(15)
					N24-C34	1.337(9)	N6-C240	1.317(16)
					N24-C21	1.354(9)	N6-C246	1.397(16)
	N-C*av*	1.471(14)	N-C*av*	1.359(14)	N-C*av*	1.355(9)	N-C*av*	1.353(15)

Symmetry transformations used to generate equivalent atoms: **1**A: x, y, −z + 1/2; 2A: −x+1, y, −z+1/2.

Crystal structure of complex 2

Complex **2** crystallizes as brown block crystals in the monoclinic $C2/c$ space group with $Z = 4$, and the ASU and its geometry is similar to that of complex **1**, but the SeCN⁻ anion is exchanged by SCN⁻ anion (Figure 2a). The Fe−N bond lengths vary from 1.959(10) Å to 1.979(10) Å with the average value of 1.969(10) Å, which are typical values for the LS Fe^{II}-N bond lengths of mononuclear Fe^{II} complex, and the C−N bond lengths vary from 1.295(14)
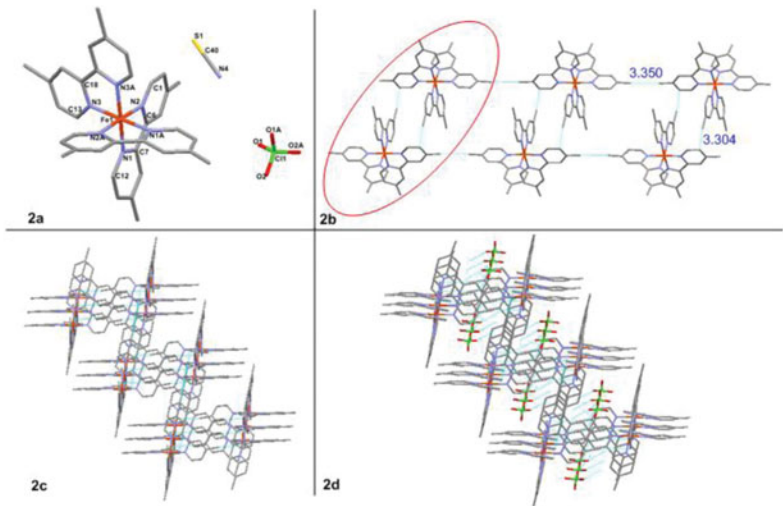

Figure 2. (a) Molecular structure and numbering scheme of complex **2**; (b) 1D chain diagram of complex **2**; (c) connecting motifs of different 1D chains; (d) 2D "stair-like" structure diagram of complex **2** with ClO_4^- anions (H atoms are omitted for clarity).
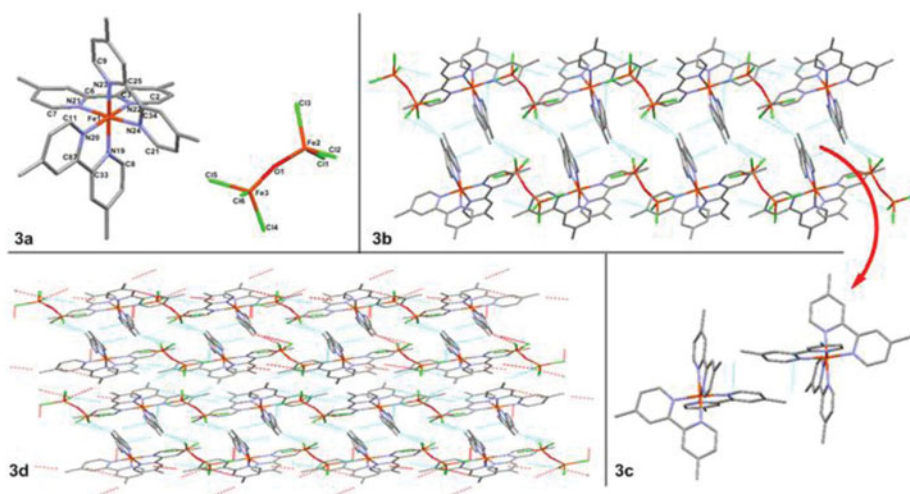
Figure 3. (a) Molecular structure and numbering scheme of complex **3**; (b) 1D chain diagram of complex **3**; (c) unit in the crystal structure of complex **3**; (d) connecting motifs of different 1D chains viewed along the *b*-axis (H atoms are omitted for clarity).

Å to 1.425(15) Å. The two pyridine rings of dmbpy are not coplanar with the dihedral angles between the same dmbpy of 7.44°, 8.27°, and 8.27° respectively. In addition, the bite angles of three dmbpy planes are 80.53, 80.53, and 88.78°.

In the crystal structure, the intermolecular short contact (distance of 3.350 Å) connects the units (circled in red line in Figure 2b) into an infinite 1D double-chain structure, and the unit consists of two cations connected by molecular interactions (distance of 3.304 Å). Different 1D double-chains are connected into a 2D "stair-like" structure through weak C-H···π contacts (Figure 2c). The dissociative ClO_4^- anions distribute evenly above and below the "steps" of the 2D "stair-like" structure (Figure 2d).

Crystal structure of complex 3

Complex **3** crystallizes as brown block crystals in the monoclinic $P2_1/c$ space group with $Z = 4$, and the ASU contains a cation and a dissociative $Fe_2OCl_6^{2-}$ anion (Figure 3a). The cation's geometry is similar to that of complex **1**, the Fe-N bond lengths vary from 1.949(6) Å to 1.987(6) Å with average value of 1.970(6) Å, and the C-N bond lengths vary from 1.336(9) Å to 1.378(9) Å. The two pyridine rings of dmbpy are not coplanar with the dihedral angles between the same dmbpy of 5.65°, 7.43°, and 10.23°, respectively. In additionally, the bite angles of three dmbpy planes are 72.12°, 83.73°, and 89.79°, compared with complexes **1**, **2**, and **4**, the $(Fe_2OCl_6)^{2-}$ anion results in more distortion of the octahedral geometry of complex **3**, which is confirmed by the selected bond angles (°) for complexes **1**–**4** in Table 3.

However, the crystal structure of complex **3** is significant different from complex **2**. The dissociative $Fe_2OCl_6^{2-}$ anions connect units of cations into an infinite 1D double-chain structure through short contacts (Figure 3b), and the unit in complex **3** consists of two cations connected by $\pi \cdots \pi$ interactions in the form of "offset face-to-face" (Figure 3c), with a vertical plane separation of 3.289 Å. The double-chains then pack parallel to each other, connected and stabilized by the dissociative $Fe_2OCl_6^{2-}$ anions via van der Waals forces (Figure 3d).

Table 3. Selected bond angles (°) for complexes **1**–**4.**

1		2		3		4	
N2-Fe1-N2A	88.9(5)	N2A-Fe1-N2	177.8(6)	N22-Fe1-N21	81.1(3)	N1-Fe7-N2	82.55(4)
N1A-Fe1-N1	79.5(6)	N2A-Fe1-N3A	87.4(4)	N22-Fe1-N23	93.6(2)	N1-Fe7-N3	94.06(4)
N2-Fe1-N3	82.6(4)	N2-Fe1-N3A	94.3(4)	N21-Fe1-N23	94.9(3)	N1-Fe7-N4	175.17(6)
N2A-Fe1-N3	96.1(4)	N2A-Fe1-N3	94.3(4)	N22-Fe1-N19	93.0(3)	N1-Fe7-N5	92.56(4)
N1A-Fe1-N3	94.7(4)	N2-Fe1-N3	87.4(4)	N21-Fe1-N19	90.6(2)	N1-Fe7-N6	93.29(6)
N1-Fe1-N3	86.7(4)	N3A-Fe1-N3	80.6(6)	N23-Fe1-N19	171.9(3)	N2-Fe7-N3	91.83(4)
N2-Fe1-N3A	95.7(4)	N2A-Fe1-N1	96.2(4)	N22-Fe1-N20	171.6(3)	N2-Fe7-N4	95.88(4)
N2A-Fe1-N3A	82.2(4)	N2-Fe1-N1	82.3(5)	N21-Fe1-N20	92.3(2)	N2-Fe7-N5	173.29(5)
N1A-Fe1-N3A	87.1(4)	N3A-Fe1-N1	174.7(4)	N23-Fe1-N20	92.2(3)	N2-Fe7-N6	93.45(4)
N2-Fe1-N1A	174.7(4)	N3-Fe1-N1	95.1(4)	N19-Fe1-N20	81.6(3)	N3-Fe7-N4	81.40(6)
N2A-Fe1-N1A	95.9(4)	N2A-Fe1-N1A	82.3(5)	N22-Fe1-N24	97.2(2)	N3-Fe7-N5	93.10(5)
N2-Fe1-N1	95.8(4)	N2-Fe1-N1A	96.2(4)	N21-Fe1-N24	175.2(2)	N3-Fe7-N6	171.44(4)
N2A-Fe1-N1	174.9(4)	N3A-Fe1-N1A	95.1(4)	N23-Fe1-N24	80.7(3)	N4-Fe7-N5	89.36(4)
N1-Fe1-N3A	95.1(4)	N3-Fe1-N1A	174.7(4)	N19-Fe1-N24	94.0(2)	N4-Fe7-N6	91.36(6)
N3-Fe1-N3A	177.6(6)	N1-Fe1-N1A	89.3(5)	N20-Fe1-N24	89.7(2)	N5-Fe7-N6	82.21(4)

Symmetry transformations used to generate equivalent atoms: (**1**A) −x, y, −z+1/2; (**2**A) −x+1, y, −z +.

Crystal structure of complex 4

Complex **4** crystallizes as brown block crystals in the monoclinic *P*2/*c* space group with *Z* = 4, and the ASU contains a cation and two dissociative BF_4^- anions (Figure 4a). The cation's geometry is similar to that of complex **1**, the Fe-N bond lengths vary from 1.922(10) Å to 2.020(10) Å with average value of 1.975(10) Å, and the C-N bond lengths vary from 1.219(14) Å to 1.443(16) Å. The two pyridine rings of dmbpy are not coplanar with the dihedral angles
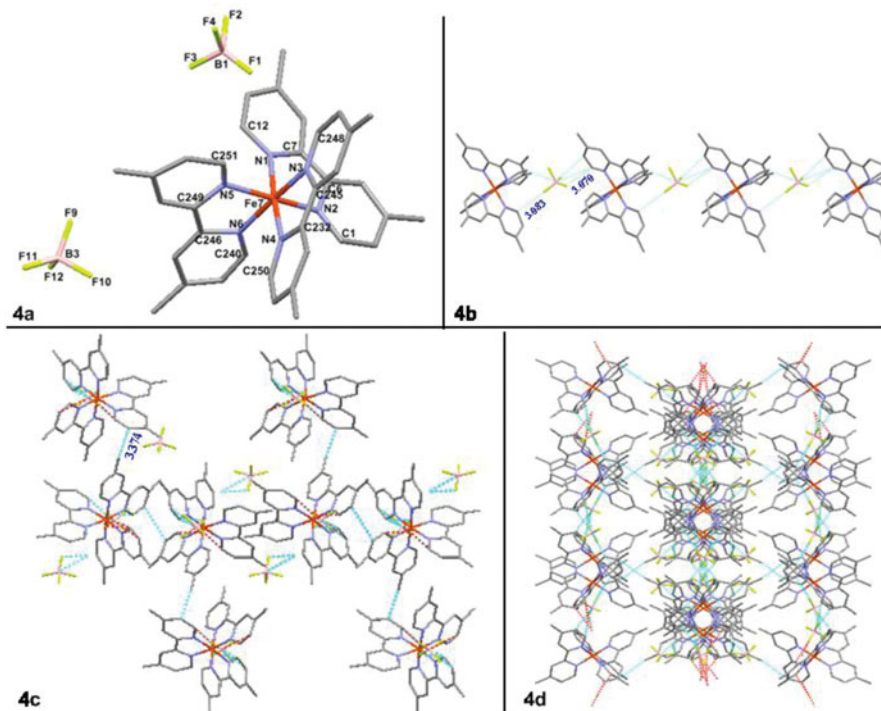

Figure 4. (a) Molecular structure and numbering scheme of complex **4**; (b) double-chain diagram of complex **4**; (c): 1D structure of complex **4** viewed along *b*-axis; (d) 1D structure viewed along *c*-axis (H atoms are omitted for clarity).
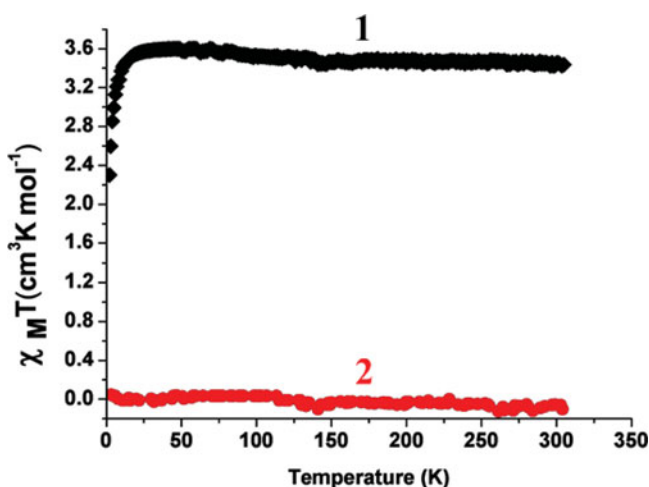
Figure 5. $\chi_M T$ versus T plots of direct current (dc) magnetic measurements of complexes **1** and **2**.

between the same dmbpy of 1.25°, 3.80°, and 4.78°, respectively. In addition, the bite angles of three dmbpy planes are 75.15°, 78.76°, and 89.56°.

In the crystal structure, the BF_4^- anions connect polycations into an infinite chain structure through C250–H250···F4 ($d_{D\ldots A} = 3.083$ Å, ∠D-H ...A = 168°) and C12–H12···F1 ($d_{D\ldots A} = 3.070$ Å, ∠D-H ...A = 173°) hydrogen bond interactions, and the two chains are connected into a double-chain structure via C287–H287···C229 ($d_{D\ldots A} = 3.374$ Å, ∠D-H ...A = 159°) weak hydrogen bond interactions (Figure 4b). Four double-chains stack parallel to each other in a staggered formation, expanding along the crystallographic b-axis to form a 1D structure via short contacts and van der Waals forces (Figure 4c). The 1D structure expands along the c-axis as shown in Figure 4d.

Magnetic properties

Temperature-dependent magnetic measurement of complexes **1** and **2** in the temperature range of 350–0 K at fields of 2 kOe are shown in Figure 5. Complex **1** shows $\chi_M T$ value 3.42 cm³ Kmol⁻¹ at room temperature, corresponding to the spin-only value of iron(II) at HS spin state. The peak value of $\chi_M T \approx 3.59$ cm³ Kmol⁻¹ at ca. 25 K, and then $\chi_M T$ drops abruptly to 2.21 cm³ Kmol⁻¹ at 2 K due to zero-field splitting. The magnetic properties of complex **2** were significantly different from that of complex **1** because of the influence of different anions. For complex **2**, it is in LS state below 305 K with $\chi_M T$ close to 0. Comparing with the Fe-N bond lengths of complex **2**, complexes **3** and **4** are in LS state as well.

Molecular Hirshfeld surfaces

The Hirshfeld surface is a useful tool for describing the surface characteristics of molecules. The 3D d_{norm} and 2D fingerprint plots of dmbpy in complexes **1**--**3** are shown in Figure 6; these clearly show the similarities and differences of the influences of different anions on the intermolecular interactions of dmbpy molecule.

The 3D molecular Hirshfeld surface is used for the identification of very close intermolecular interactions. The value of d_{norm} is negative or positive when intermolecular contacts are shorter or longer than r_{vdW} (van der Waals (vdW) radii). The d_{norm} values are mapped onto the
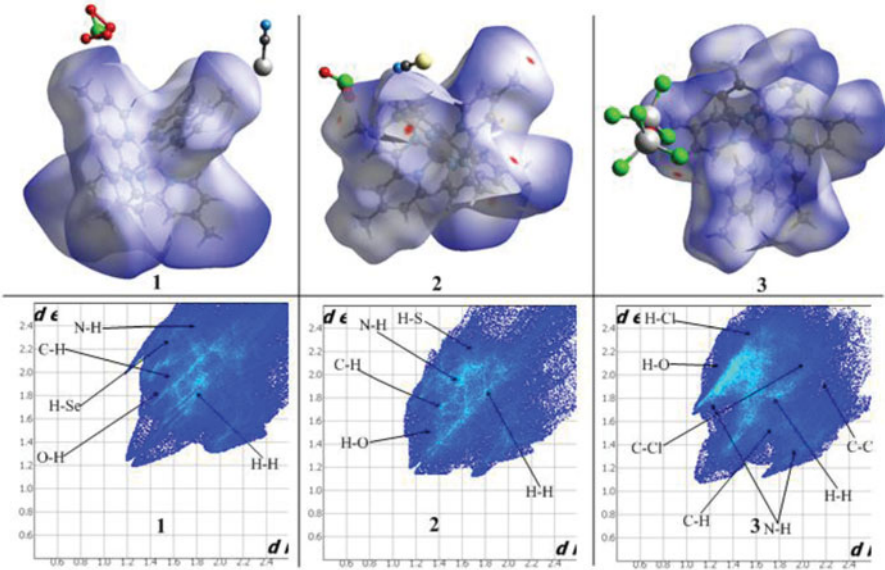
Figure 6. The 3D molecular Hirshfeld d_{norm} surfaces and 2D fingerprint plots of dmbpy in complexes **1**–**3**.

Hirshfeld surface by using a red–blue–white color scheme: red regions correspond to closer contacts and negative d_{norm} value; blue regions correspond to longer contacts and positive d_{norm} value; and white regions correspond to the distance of contacts that is exactly the vdW separation and with a d_{norm} value of zero. Figure 6 clearly shows that the vdW forces and longer contacts account for the total Hirshfeld surfaces except that only small red regions in complexes **2** and **3** on the d_{norm} surfaces correspond to significant C−H ⋯ π interactions and $\pi \cdots \pi$ interactions, respectively.

The 2D fingerprint plots complement the Hirshfeld surface; these are quantitatively summarizing the nature and type of intermolecular contacts experienced by the molecules in the crystal. The main intermolecular contacts are H−H contacts, which are reflected in the middle of scattered points in the 2D fingerprint plot and are similar in three complexes (Table 4). Compared with complexes **1** and **2**, the percentage of N−H and C−H interactions in complex **3** declined, especially the O−H interactions decreased dramatically. This phenomenon may be attributed to the significant existence of H-Cl interactions in complex **3**. The C−C interactions have a significant contribution to the total Hirshfeld surfaces of complex **3**, comprising 1.3%, which is larger than complexes **1** and **2**, corresponding to the existence of $\pi \cdots \pi$ interactions in complex **3**.

Apart from the above, the presence of N−C, C−O, C−Se, H−Se, C−S, H−S, H−Fe, and C−Cl contacts are observed, and are summarized in Table 4. The most closet contacts for dmbpy in complexes **1**–**3** (N-Fe contacts) cannot be included in Table 4 due to the fact that the Hirshfeld analysis is only concerned with intra-molecular interactions and intermolecular interactions should not be considered. It is interesting that for the two coordinate N atoms of one receptor,

Table 4. Summary of various contact contributions to the dmbpy Hirshfeld surface area in complexes **1**–**3**.

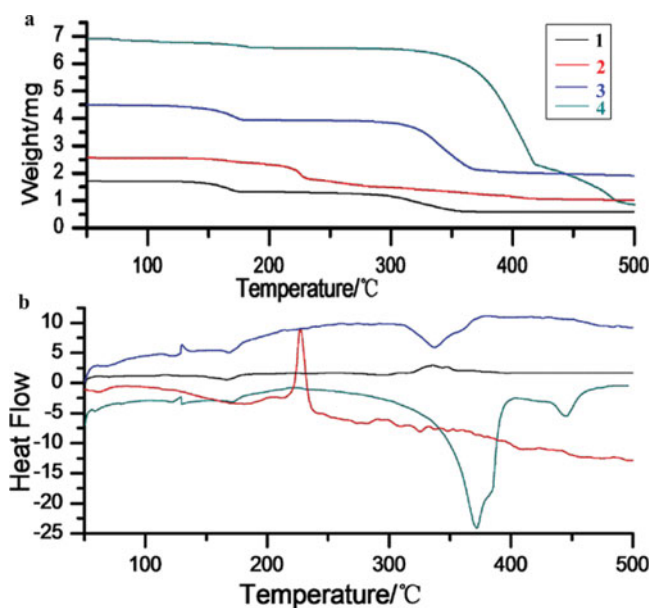|	H-H	N-H	C-H	O-H	H-Cl	N-C	C-C	C-O	C-Se	H-Se	C-S	H-S	H-Fe	C-Cl
1.	42.0	3.2	22.4	11.4	0.2	0.6	0.1	0.2	0.2	4.0	0	0	0	0
2.	44.2	3.9	23.4	12.8	0	0	0.3	0.4	0	0	0.6	3.3	0	0
3.	44.2	2.1	20.8	2.0	25.9	0	1.3	0	0	0	0	0	0.4	2.6

Figure 7. (a) TGA, and (b) DSC profiles of complexes **1–4**.

only one dmbpy molecule in complex **2** shows the identical bond length between Fe ion and the two coordinate N atoms. In addition, the average values of N-Fe bonds vary from 1.969 Å to 2.131 Å, which may be attributed to the difference in anions, resulting in different spin states among the complexes.

Thermal study

The thermal behaviors of complexes **1–4** were investigated on a STAR^e System (from Mettler–Toledo), and were heated at a rate of 10°C per minute with a temperature range of 50–500°C. Figure 7 shows the TGA and DSC traces of these.

   Almost identical thermal decomposition processes can be observed in complexes **1** and **3**, the first weight loss of 22.67% and 19.54% at 110–180°C corresponding to the removal of one dmbpy molecule (calculated values are 21.78% and 19.41%). The second weight loss above 240°C is due to the decomposition of other two dmbpy ligands with a mass loss of 44.20% and 40.94% (calculated values are 45.32% and 38.83%) to give the Fe(ClO$_4$)(SeCN) and Fe(Fe$_2$OCl$_6$) residue, respectively. Compared with complexes **1** and **3**, four main thermal decomposition processes can be observed for complex **2**. From 130°C to 185°C, the first weight loss of 7.12% (calculated value is 7.57%) is due to the decomposition of SCN$^-$ anion. The second weight loss of 22.47% and the last weight loss of 21.95% (calculated value is 24.05%) at 190–230°C and 300–430°C are attributed to the removal of dmbpy molecule. From 230°C to 290°C, the weight loss of 11.91% (calculated value is 12.98%) is due to the decomposition of ClO$_4^-$ anion, and there is an aiguille with the peak temperature of 231°C in the DSC profile of complex **2**, which may be due to the explosion of ClO4$^-$ anion. In the TGA trace of complex **4**, no weight loss was observed up to 280°C; however, an abrupt weight loss was observed in a temperature range of 280–400°C because of the decomposition of two dmbpy ligands with a mass loss of 50.09% (the calculated value is 47.11%). The second weight loss of 22.14% at 400–470°C is due to the removal of the remaining dmbpy ligand to give

$Fe(BF_4)_2$ residue. The thermal decomposition features of these are in good agreement with their crystal structures.

Conclusions

In conclusion, the influence of different anions $[(ClO_4)^-(SeCN)^-$, $(ClO_4)^-(SCN)^-$, $(Fe_2OCl_6)^{2-}$, and $BF_4^-]$ on the crystal structures, magnetic properties, and intermolecular interactions of complexes **1–4** has been investigated. The $(ClO_4)^-(SeCN)^-$ anion leads to the longest Fe-N bond lengths with an average value of 2.131 Å, and the $(ClO_4)^-(SCN)^-$ anion leads to the shortest N-Fe bond lengths with an average value of 1.969 Å, and correspondingly complex **1** is in HS state and complex **2** is in LS state. Moreover, $(ClO_4)^-(SCN)^-$ and $(Fe_2OCl_6)^{2-}$ anions resulting in complexes **2** and **3** have C-H$\cdots\pi$ and $\pi\cdots\pi$ interactions in their crystal structures, respectively. In complex **4**, BF_4^- leads to the crystal structure stabilized via C-H$\cdots$F and C-H$\cdots$C hydrogen bond interactions, and the thermal studies revealed that complex **4** was more stable than the other complexes. In complex **3**, the $(Fe_2OCl_6)^{2-}$ anion generates more distortional octahedral geometry of cation than other anions.

Funding

Supplemental information

CCDC reference numbers 992727, 998998, and 990506 contain the supplementary crystallographic data in CIF format for complexes **1–3** reported in this paper, respectively.

References

[1] Delbari, A. S., Shahvelayati, A. S., Jodaian, V., & Amani, V. (2014). *J. Iran. Chem. Soc.*, *12*, 223.
[2] (a) Huang, W., & Ogawa, T. (2006). *J. Mol. Struct.*, *785*, 21. (b) Luo, Y. H., Liu, Q. L., Ling, Y., Yang, L. J., Wang, W., & Sun, B. W. (2014). *Inorganica Chimica Acta*, *425*, 255.
[3] Ghiasi, Z., Amani, V., Mirzaei, P., Safari, N., & Abedi, A.. (2013). *Aust. J. Chem.*, *66*, 676.
[4] Alizadeh, R., Mohammadi Eshlaghi, P., & Amani, V.. (2010). *Acta Crystallogr.*, *E66*, m996.
[5] Albada, G. A., Mutikainen, I., Roubeau, O., Turpeinen, U., & Reedijk, J. (2002). *Inorg. Chim. Acta*, *331*, 208.
[6] Willett, R. D., Pon, G., & Nagy, C. (2001). *Inorg. Chem.*, *40*, 4342.
[7] Constable, E. C., Husecroft, C. E., Neuburger, M., Poleschak, I., & Zehnder, M. (2003). *Polyhedron*, *22*, 93.
[8] Wehman, P., Dol, G. C., Moorman, E. R., Kamer, P. C. J., van Leeuwen, P. W. N. M., Fraanje, J., & Goubitz, K. (1994). *Organometallics*, *13*, 4856.
[9] Onggo, D., & Goodwin, H. A. (1991). *Aust. J. Chem.*, *44*, 1539.
[10] Ksenofontov, V., Levchenko, G., Spiering, H., Gutlich, P., Letard, J. F., Bouhedja, Y., & Kahn, O. (1998). *Chem. Phys. Lett.*, *294*, 545.
[11] Lara, F. J. M., Gaspar, A. B., Aravena, D., Ruiz, E., Muñoz, M. C., Ohba, M., Ohtani, R., Kitagawa, S., & Real, J. A. (2012). *Chem. Commun.*, *48*, 4686.
[12] Menage, S., Vincent, J. M., Lambeaux, C., Chottard, G., Grant, A., & Fontecave, M. (1993). *Inorg. Chem.*, *32*, 4766.
[13] Pomeranc, D., Heitz, V., Chambron, J. C., & Sauvage, J. P. (2001). *J. Am. Chem. Soc.*, *123*, 12215.
[14] Oshio, H., Yamamoto, M., & Ito, T. (2001). *Inorg. Chem.*, *41*, 5817.
[15] Luo, Y. H., Yang, L. J., Liu, Q. L., Ling, Y., Wang, W., & Sun, B. W. (2014). *Dalton Trans.*, *43*, 16937.

[16] Amani, V., Abedi, A., Ghabeshi, S., Khavasi, H. R., Hosseini, S. M., & Safari, N. (2014). *Polyhedron*, *79*, 104.
[17] Luo, Y. H., Song, W. T., Ge, S. W., & Sun, B. W.. (2014). *Polyhedron*, *69*, 160.
[18] Rigaku. (2005). *Crystal Clear, Version 14.0*, Rigaku Corporation: Tokyo, Japan.
[19] Sheldrick, M. (1997). *SHELXS97: Programs for Crystal Structure Analysis*, University of Göttingen: Göttingen, Germany.
[20] Luo, Y. H., & Sun, B. W. (2014). *Spectrochimica Acta A*, *120*, 381.
[21] CCDC. (2003). *Mercury 2.3 Supplied with Cambridge Structural Database*, CCDC: Cambridge, UK.
[22] (a) Wolff, S. K., Grimwood, D. J., McKinnon, J. J., Jayatilaka, D., & Spackman, M. A. (2007). *CrystalExplorer 2.0.* University of Western Australia: Perth, Australia. (b) Luo, Y. H., Ge, S. W., Song, W. T., & Sun, B. W. (2014). *New J. Chem.*, *38*, 723. (c) Luo, Y. H., Wu, D. E., Ge, S. W., Li, Y., & Sun, B. W. (2014). *RSC Adv.*, *4*, 11698.